MRS Advances (2023) 8:645–650
https://doi.org/10.1557/s43580-023-00573-7

ORIGINAL PAPER

First-principles study of $Ti_{50}Ru_{50-x}Y_x$ (Y = Ni, Pd and Pt) with a prospect to induce SME on stable CsCl-type $Ti_{50}Ru_{50}$ phase

B. S. Ngobe[1,2] · M. J. Phasha[1] · M. P. Molepo[2] · I. A. Mwamba[1]

Received: 3 February 2023 / Accepted: 15 April 2023 / Published online: 31 May 2023

Abstract

Most CsCl-type intermetallics composed of group IV and VIII–XI transition metals have shape memory effect (SME), a phenomenon that occurs on a certain class of materials with an ability to undergo martensitic transformation (MT) during cooling. This advanced functional materials' property is enabled by MT from high-temperature B2 phase of high symmetry to lower symmetry phases such as $L1_0$, B19 or B19' upon cooling. Peculiarly, $Ti_{50}Ru_{50}$ with similar ordered B2 at high temperature remains ordered and stable with no phase transition down to room temperature. In this study, first-principles calculations based on density functional theory (DFT) are used to investigate the structural, thermodynamic and electronic properties of the stable $Ti_{50}Ru_{50}$ compound by systematically substituting part of the Ru atoms with ductile group 10 metal (Ni, Pd and Pt). This is an attempt to destabilizing B2 phase at 0 K through $Ti_{50}Ru_{50-x}Y_x$ ternary alloying to promote MT that could yield SME.

Introduction

The Cesium Chloride (CsCl) intermetallic formed at composition near 50:50 atomic percentage (at. %) is one of the prominent features in Ti-based intermetallics [1–4]. This B2 phase forms congruently at a high temperature [2, 3]. In most systems, this high-symmetry crystal structure becomes unstable on cooling and undergoes phase transformation to low-symmetry martensite phases that are stable at lower temperatures such as orthorhombic-B19 ($Ti_{50}Pd_{50}$ and $Ti_{50}Pt_{50}$) and monoclinic-B19′ ($Ti_{50}Ni_{50}$) characterized by shape memory effects (SME) [1, 5].

MT is one of the key characteristics of shape memory alloys (SMAs), a class of materials with the ability to remember their prior shape upon re-heating [6]. This material's behaviour has been observed in Nitinol ($Ti_{50}Ni_{50}$) alloys that are used in high-tech products such as robotic arms, temperature-sensing actuators and eyeglass frames because of their superior shape memory effect and super-plasticity [1, 7]. The maximum MT temperature of 373 K hinders Nitinol for use in high-temperature applications [1, 8].

✉ B. S. Ngobe
bonganing@mintek.co.za

1 Advanced Materials Division, Mintek, Private Bag X 3015, Randburg 2125, South Africa

2 School of Physics, University of the Witwatersrand, Private Bag 3, Wits 2050, Johannesburg, South Africa

Thus, SMAs containing platinum group metals (PGMs) such as $Ti_{50}Pd_{50}$ and $Ti_{50}Pt_{50}$ are pursued to overcome Nitinol operational limitation [2, 3, 6]. However, the high cost of PGMs renders the selection uneconomical for potential high-temperature SMAs (HTSMAs). Ruthenium (Ru) is the cheapest and most readily available among the PGMs, mostly used in chemical and electronics industries [9]. If added to Ti alloys and other super-alloys such as those applied in the aerospace industry, Ru improves corrosion resistance and chemical and electrical stability at higher temperatures [10]. In addition, TiRu binary system consisting of a B2 phase is currently explored for hydrogen storage applications [6]. However, since B2 $Ti_{50}Ru_{50}$ remains stable on cooling to low temperatures [11], it cannot be considered for shape memory applications in its pristine form.

This research work aims to use first-principles calculations to investigate the effect of alloying on B2 $Ti_{50}Ru_{50}$ by computing the thermodynamic, electronic and elastic properties. The aforementioned will enable us to explore the possibility of inducing MT of the stable B2 $Ti_{50}Ru_{50}$ by systematically introducing alloying element Y (Y = Ni, Pd and Pt) on the Ru site to predict properties of B2 ternary $Ti_{50}Ru_{50-x}Y_x$ compositions which could bear SME.

Shape memory behaviour is sensitive to compositional change. Consequently, a virtual crystal approximation (VCA) was employed to conduct alloying at "**x**" composition range from 0, 2.5 to 10, 15, 25 and 50 at. %. A similar DFT-VCA approach was used in our previous research work [12], where

focus was only limited to Pd. In this work, a similar solid-solution unit cell approach is used to investigate the effect of Ni and Pt and compared to that carried on Pd alloying.

Computational methodology

The calculations reported here were carried out using the DFT-based CASTEP code [13]. The ultra-soft pseudopotentials were used to model the electron–ion interactions [14]. Furthermore, the electron-exchange correlation was described by the Perdew–Burke–Ernzerhof (PBE) functional of the generalized gradient approximation (GGA) [15] since it gives the best estimates of the lattice parameters as compared to theoretical or experimental findings of the binary compounds. Cut-off energy of 500 eV and the k-points of $13\times13\times13$ were used and found to be sufficient enough to converge the total energy of the investigated B2 compounds.

All the equilibrium B2 crystal structures were obtained through geometry optimization in the Brayden–Fletcher–Goldfarb–Shanno (BFGS) minimization scheme [16]. The convergence criterion of less than 1×10^{-5} eV/atom, the maximum residual forces of 0.03 eV/Å, the maximum residual bulk stress of 0.05GPa and the maximum atomic displacement of 1×10^{-3} Å were utilized to achieve maximum accuracy.

Figure 1a–c shows the schematic representation of the crystal structure used to carry the thermodynamic, mechanical and electronic properties of the investigated structures.

Results and discussion

Structural and thermodynamic properties

The investigated structures that are shown in Fig. 1a–c were optimized first to obtain their equilibrium ground state; thereafter, all other properties were computed from these structures. Figure 2a–c presents the equilibrium lattice parameters, while d–f presents the enthalpies of the formation of the investigated compositions. To benchmark our model's accuracy, we calculated and compared the lattice parameters of pristine $Ti_{50}Y_{50}$ (Y = Ni, Ru, Pd and Pt) to that of the literature. The results of binary alloys presented in Fig. 2a–c were found to agree with data found in the literature to within the tolerance margins of 3% [6, 7, 11, 17–19]. However, to the best of the authors' knowledge, there are no other studies conducted previously on these ternaries ($T_{50}Ru_{50-x}Y_x$) using the VCA approach to compare current results with, indicating the novelty of this study.

Figure 2a–c shows that as expected, the partial substitution by Ni on the Ru atom site decreases the lattice parameter whereas Pd and Pt increase the lattice parameter. This is attributed to the atomic radii difference, with Ni having a smaller atomic radius than Ru while Pd and Pt have a larger atomic radius.

The enthalpy of formation (ΔH_F) as expressed in Eq. 1, [20], is used to determine the thermodynamic ability of a compound to form.

$$\Delta H_f = \left\{ \frac{1}{2} E_T^{Ti_{50}Ru_{50-x}Y_x} - xE_{sol}^{Ti} - (1-x)E_{sol}^{Ru_{50-x}-Y_x} \right\}, \quad (1)$$

where E_T^{TiRuY} represents the energy of the B2 compound, $E_{Element}^{Ti}$ and $E_{Element}^{Ru-Y}$ represent the elemental energies of Ti and Ru-Y in their ground state. A phase is stable if $\Delta H_F < 0$, else unstable at 0 K if $\Delta H_F > 0$ [21]. Figure 2d–f shows that all the investigated structures were found to be negative, indicating thermodynamic stability. Our benchmarked binaries were found to be in accordance with the results reported by other authors [18, 20, 22, 23]. In Fig. 2d–f, one can ascertain that the addition of Y atoms on the Ru site in less than 15 at.% seems to increase the thermodynamic stability of the ternaries when compared to $Ti_{50}Ru_{50}$, but in general, the stability starts to decrease as Y composition is at 15 at.% and above.

Electronic properties

The total density of states (TDOS) is used to predict electronic stability by observing the position of the Fermi level ($E\text{-}E_F = 0$) to the pseudogap, which can be used to interpret the stability of a phase [12, 24]. Figure 3a–c shows the TDOS of the investigated compositions. All the compositions reported in this work were found to be non-zero around the Fermi level, indicating metallic bonding. For pristine compounds, the valence and the conduction band of $Ti_{50}Ru_{50}$ were found to coincide perfectly at the fermi level resulting in a deep valley, indicating that it is the most stable

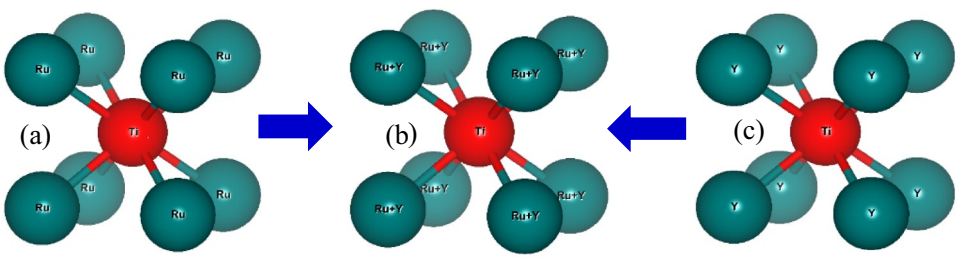

Fig. 1 Crystallographic view of B2 **a** $Ti_{50}Ru_{50}$, **b** $T_{50}Ru_{50-x}Y_x$ and **c** $Ti_{50}Y_{50}$ structures, where Y represents Ni, Pd and Pt

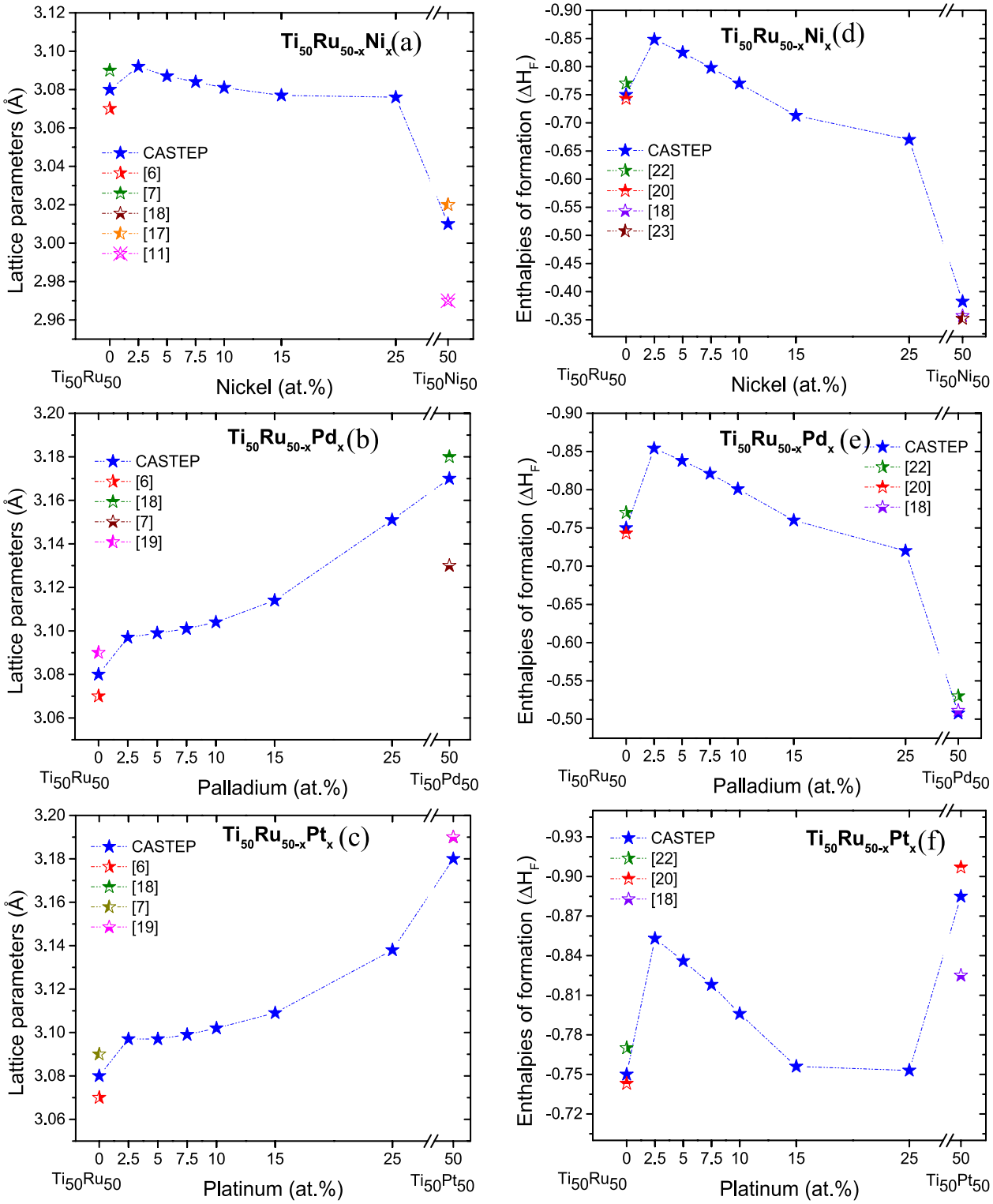

Fig. 2 Equilibrium lattice parameters **a**–**c** and enthalpies of formation **d**–**f** of $T_{50}Ru_{50-x}Y_x$ alloys

structure. However, E-E_F for $Ti_{50}Ni_{50}$, $Ti_{50}Pd_{50}$ and $Ti_{50}Pt_{50}$ were found to shift the pseudogap towards the conduction band, indicating phase transition tendency. It can also be noted that the addition of Y (Ni, Pd and Pt) atoms on the Ru site altered the valence-conduction bands co-existence at the fermi level. This shifted the deep valley towards the

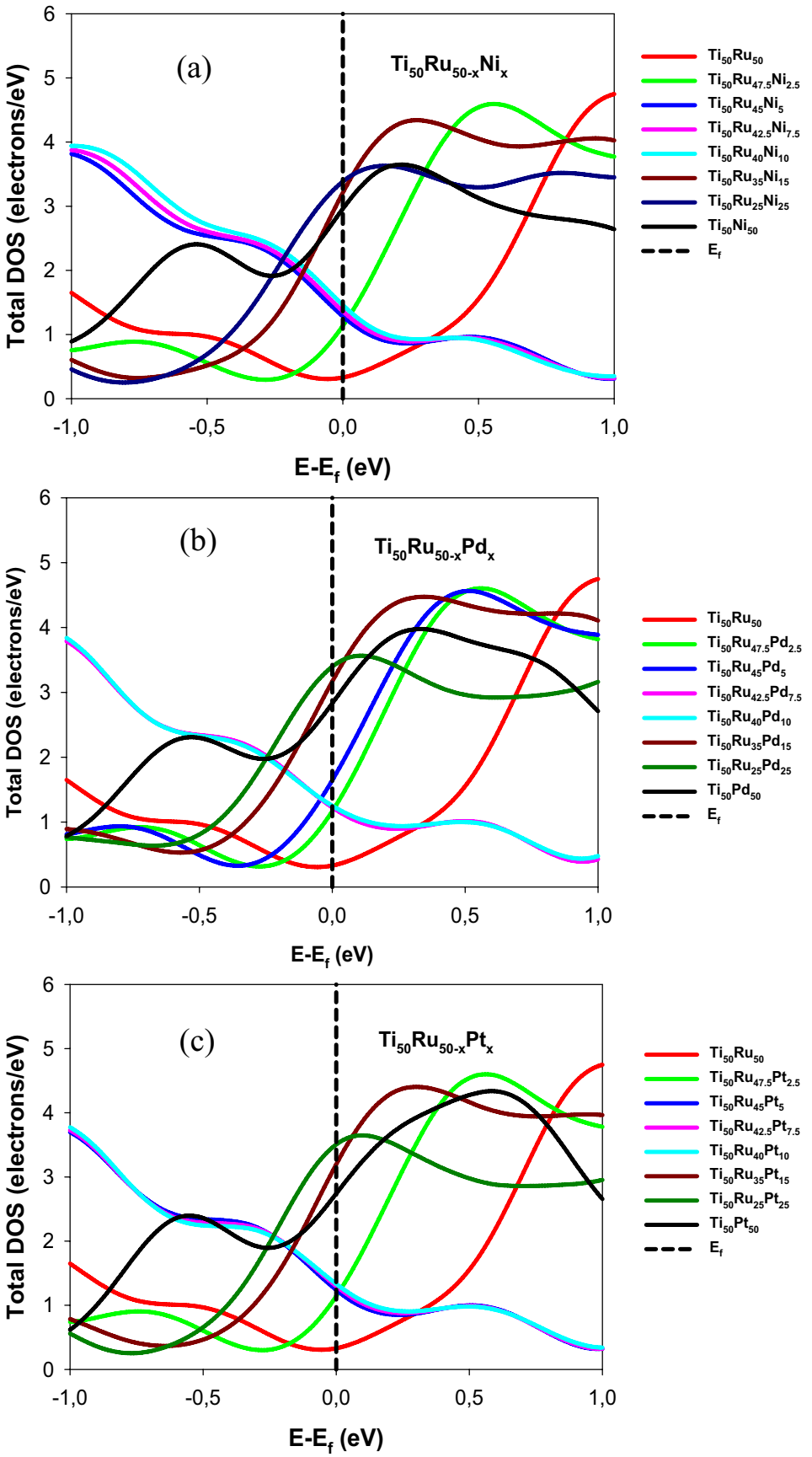

Fig. 3 The total density of states of the investigated structures **a** $Ti_{50}Ru_{50-x}Ni_x$, **b** $Ti_{50}Ru_{50-x}Pd_x$ and **c** $Ti_{50}Ru_{50-x}Pt_x$. The Fermi energy is taken as energy zero ($E–E_F=0$)

conduction band, rendering the subsequent phase unstable with the potential to undergo a phase transition.

Elastic properties and mechanical stability

The mechanical stability of a crystal structure can be determined from the computed elastic constants (C_{ij}) [25]. For a cubic system, there are only three independent elastic constants, namely, C_{11}, C_{12} and C_{44}. Born-Huang's lattice dynamical theory [26] states that the cubic mechanical stability criterion can be endorsed by satisfying all the impartialities given in Eq. 2.

$$C_{11} > 0, C_{44} > 0, C_{11} - C_{12} > 0, C_{11} + 2C_{12} > 0. \quad (2)$$

A shear elastic coefficient (C') for assessing the compound's prospect to undergo phase transition (as a way of ascertaining the phase stability or instability) at 0 K can be expressed as shown in Eq. 3:

$$C' = \left(\frac{C_{11} - C_{12}}{2}\right). \quad (3)$$

The mechanical stability of a crystal decreases when approaching the phase transition [27], this is at the point where C' becomes smaller than the trigonal shear constant (C_{44}) which represents the crystal's rigidity against shearing. A negative C' signifies features of SMAs that are capable of operating at high-temperature conditions [28]. Figure 4a–c shows the elastic constants of the investigated B2 compositions. For pristine binary compounds, both $Ti_{50}Ru_{50}$ and $Ti_{50}Ni_{50}$ upheld the Born criteria, while $Ti_{50}Pd_{50}$ and $Ti_{50}Pt_{50}$ did not comply with the criteria ($C_{11} < C_{12}$), signifying instability at 0 K. Figure 4a–c further shows that $C_{44} > C'$ and C' closer to 0 for $Ti_{50}Ni_{50}$, indicating likeliness

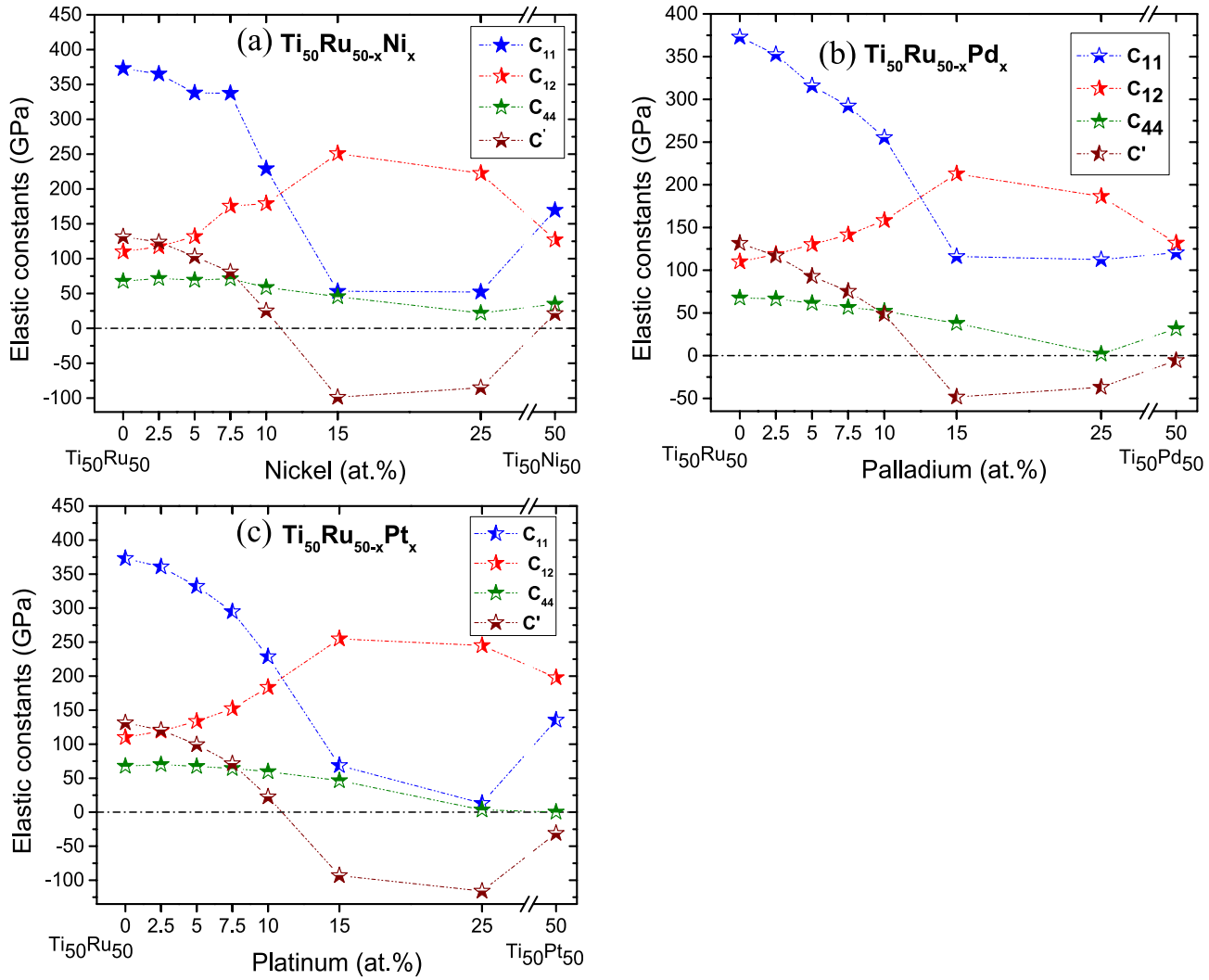

Fig. 4 The elastic constants (Cij) of $Ti_{50}Ru_{50-x}Y_x$ ($x = 0$, 2.5–10, 15, 25 and 50 at. %) where Y represent **a** Ni, **b** Pd and **c** Pt

to undergo a phase transition. Although $Ti_{50}Pd_{50}$ and $Ti_{50}Pt_{50}$ compounds were both found prone to undergo a phase transition at higher temperatures ($C' < 0$), the C' value of $Ti_{50}Pt_{50}$ was found to be the lowest, signalling the highest MT temperature, consistent with theoretical [28] and experimental data [5] in the literature.

Furthermore, in all the investigated ternaries, at compositions above 10 at. %, the Born criteria are not upheld, predicting that SME could be induced in these $T_{50}Ru_{50-x}Y_x$ ternary compositions. The features of HTSMA's prospects can also be deduced on 15–50 at. % Y composition range where C′ is found to be negative, with $Ti_{50}Ru_{25}Pt_{25}$ is found to be the most negative of all compositions studied.

Conclusion

The DFT model choice used in this research work showed greater consistency and reliability. The structural parameters of the pristine binary alloys were found to agree with data in the literature. The results obtained affirm the theoretical observation that B2 $Ti_{50}Ru_{50}$ phase remains stable with no phase transition down to 0 K. As proclaimed in the literature, C' for both $Ti_{50}Pd_{50}$ and $Ti_{50}Pt_{50}$ was found negative, indicating high-temperature phase transformation tendency features. The DOS also found $Ti_{50}Ru_{50}$ stable with valence and conduction bands coinciding at the centre of the pseudogap, while E_F of $Ti_{50}Pd_{50}$ and $Ti_{50}Pt_{50}$ shifted towards the conduction band. The addition of Y atoms above 10 at. % was able to ensure $C' < 0$ and shifts pseudogap towards the conduction band. This study successfully identified $T_{50}Ru_{50-x}Y_x$ ternary alloy compositions in which SME can be induced.

Acknowledgments This paper is published with the permission of MINTEK and The University of the Witwatersrand. The authors would like to thank the Advanced Metals Initiative (AMI) of the Department of Science and Innovation (DSI) of South Africa for financial support. In addition, Dr Maje Phasha is grateful for financial support from the National Research Foundation (NRF) of South Africa—JSPS GRANT No: 148782. Finally, the gratitude is further extended to the Centre for High-Performance Computing (CHPC) in Cape Town for allowing us to carry out the computational calculations using their remote computing resources.

Funding Open access funding provided by Mintek.

Data availability Reasonable data can be made available on request from the corresponding authors.

Declarations

Conflict of interest The authors declares no conflict of interest.

References

1. A. Wadood, HEC, pp. 1–144 (2018).
2. S.E. Kulkova, D.V. Valujsky, J. Phys. IV **11**, 53–58 (2001)
3. S.E. Kulkova, D.V. Valujsky, J.S. Kim, G. Lee, Y.M. Koo, Solid State Commun. **119**, 619–623 (2001)
4. H. Baker, *ASM handbook, 10th edn. Alloy phase diagrams*, vol. 3 (ASM International, Detroit, 1992), pp.1340–1378
5. H. Donkersloot, J.V. Vucht, JLCM **20**, 83–91 (1970)
6. Z.Z. Kong, Y.H. Duan, M.J. Peng, D.Y. Qu, L.K. Bao, Physica. B Cond. Matter. **573**, 13–21 (2019)
7. W. Bao, D. Liu, Y. Duan, M. Peng, Philos. Mag. **99**, 1–22 (2019)
8. A. Wadood, Adv. Mate. Sci. Eng. **2016**, 1–9 (2016)
9. E. Jain, G. Pagare, S.S. Chouhan, S.P. Sanyal, Intermetallics **54**, 79–85 (2014)
10. L.A. Cornish, J.S. Afr, Inst. Min. Metall. **117**, 969–974 (2017)
11. R. John, H. Ruben, Mater. Sci. Appl. **2**, 1355–1366 (2011)
12. B.S. Ngobe, M.J. Phasha, I.A. Mwamba, SAJST **40**, 205–211 (2021)
13. S.J. Clark, M.D. Segall, C.J. Pickard, P.J. Hasnip, M.I. Probert, K. Refson, M.C. Payne, Z. Kristallogr. **220**, 567–570 (2005)
14. D. Vanderbilt, Phys. Rev. B **41**, 7892–7895 (1990)
15. J.P. Perdew, K. Burke, M. Ernzerhof, Phys. Rev. Lett. **77**, 3865–3868 (1996)
16. T. Fischer, J. Almlof, J. Phys. Chem. **96**, 9768–9774 (1992)
17. T. Philip, P. Beck, Trans. AIME. **209**, 1269–1271 (1957)
18. J. Jung, G. Ghosh, G. Olson, Acta Mater. **51**, 6341–6357 (2003)
19. A. Wadood, Y. Yamabe-Mitarai, Platinum Metalls Rev. **58**, 61–67 (2014)
20. W.W. Xing, X.Q. Chen, D.Z. Li, L.Y. Li, C.L. Fu, Intermetallics **28**, 16–24 (2012)
21. J. Yang, J.H. Huang, Z. Ye, D.Y. Fan, S.H. Chen, Y. Zhao, Ceram Int. **43**, 7751–7761 (2017)
22. E. Semenova, Powder. Metall. MCeram. **36**, 394–404 (1997)
23. J.G. Gachon, N. Selhaoui, B. Aba, J. Hertz, J. Phase Equilibria. **13**, 506–511 (1992)
24. P. Ravindran, R. Asokamani, Bull. Mater. Sci. **20**, 613–622 (1997)
25. S.C. Wu, G.H. Fecher, S.S. Naghavi, C. Felser, J. Appl. Phys. **125**, 082523-1–0825231-8 (2019)
26. O. Gomisa, F.J. Manjónb, P. Rodríguez-Hernándezc, A. Muñozc, J. Phys. Chem. Solids **124**, 111–120 (2019)
27. P. Sedlák, M. Janovská, L. Bodnárová, O. Heczko, H. Seiner, Metals **10**, 1–13 (2020)
28. R.G. Diale, R. Modiba, P.E. Ngoepe, H.R. Chauke, MRS Adv **4**, 2419–2429 (2019)